JOURNAL OF CATALYSIS **171,** 93–105 (1997)
ARTICLE NO. CA971781

Kinetics of the Selective CO Oxidation in H_2-Rich Gas on Pt/Al_2O_3

M. J. Kahlich, H. A. Gasteiger,[1] and R. J. Behm

Abteilung Oberflächenchemie und Katalyse, Universität Ulm, D-89069 Ulm, Germany

Received December 20, 1996; revised May 7, 1996; accepted June 2, 1997

The selective CO oxidation reaction on Pt/γ-Al_2O_3 in simulated reformer gas (75% H_2; the rest is N_2) was investigated over a wide range of CO concentrations (0.02–1.5%) at low stoichiometric O_2 excess ($p_{O_2}/p_{CO} = 0.5$–1.5). Integral flow measurements in a microreactor showed that the optimum temperature for the PROX process (preferential oxidation) was ~200°C; rates of CO methanation in this range were insignificant. At higher temperatures a significant loss in selectivity was observed. The quantitative determination of CO oxidation rates and selectivities as a function of CO and O_2 concentration between 150 and 250°C by differential flow measurements led to reaction orders of −0.4 for p_{CO} and +0.8 for p_{O_2} at an apparent activation energy of 71 kJ/mol. These kinetics are consistent with the selective CO oxidation reaction occurring in the *low-rate branch*, on a surface predominantly covered with adsorbed CO. Its ramifications on the observed dependence of the selectivity on both CO concentration and temperature are discussed. A H_2-induced increase in the CO oxidation rate by a factor of ~2 was observed. Comparison of the kinetic rate expression for the selective CO oxidation with the performance of a plug-flow reactor (variable flow rates) led to quantitative agreement.

1. INTRODUCTION

The selective oxidation of CO in a H_2-rich atmosphere (PROX (1)) has long been of considerable technical interest for purification of hydrogen feed gas, e.g., for H_2 supply in ammonia synthesis. Over the last years, the PROX process has attracted new interest due to its use in fuel cell technology. To avoid the issue of hydrogen distribution and storage for H_2-PEM fuel cells (*polymer electrolyte membrane*), in particular in vehicle applications, H_2 can be produced locally (*on-board*) by steam reformation of methanol (2). The resulting gas mixture (reformer gas) of ~75% H_2 in ~25% CO_2 is, however, contaminated with 1–2% CO (1, 3, 4). Unfortunately, trace amounts of CO in the H_2-PEMFC effect a devastating deterioration of the energy conversion efficiency of the fuel cell *via* CO-induced poisoning of the anode catalyst and, therefore, the maximum acceptable CO concentration for *state of the art* Pt–Ru electrodes is ≤100 ppm (5).

Considering the problems associated with other methods for CO removal (methanation and membrane-based processes (1, 6, 7)), the selective oxidation of CO seems to be the most straightforward method to reduce the CO contamination in the reformate down to the ppm-level. The crucial requirements for the PROX reaction are high CO oxidation rate and, equally important, high selectivity, S. The latter is defined as the ratio of oxygen consumption for the CO oxidation reaction (to CO_2) over the total oxygen consumption, which includes the oxygen loss due to H_2 oxidation (to H_2O):

$$S = \frac{\Delta O_2^{(CO)}}{\Delta O_2^{(CO)} + \Delta O_2^{(H_2)}}. \qquad [1]$$

The formation of water reduces the amount of hydrogen which can be fed into the fuel cell, so that the selectivity must be large enough to not reduce the fuel efficiency of the overall system. For example, a selectivity of 50% implies that equal amounts of CO_2 (desired reaction) and H_2O (side reaction) are being produced, equating to a loss of approximately 2.7% in fuel efficiency for typically 2% vol CO in the reformate. Similar losses of hydrogen can also be caused by other side reactions, *viz*., the methanation of both CO and CO_2.

The oxygen excess with respect to the amount of oxygen required for the oxidation of CO to CO_2 is commonly characterized by the process parameter λ:

$$\lambda = \frac{2c_{O_2}}{c_{CO}} = \frac{2p_{O_2}}{p_{CO}}, \qquad [2]$$

where $\lambda = 1$ is sufficient to provide for the complete oxidation of CO to CO_2 in the absence of an oxygen-consuming side reaction (H_2 oxidation). A comparison of Eqs. [1] and [2] demonstrates that S and λ are interrelated; process conditions which yield a selectivity of 50% will afford a complete conversion of CO to CO_2 if the λ-value at the reactor entrance is ≥2. In other words, the lower the selectivity of the process, the higher will be the λ-value required to completely oxidize CO to CO_2.

[1] Corresponding author. Fax: +49-(731)-502-5452. E-mail: hubert.gasteiger@chemie.uni-ulm.de.

0021-9517/97 $25.00

Catalysts proposed for the selective CO oxidation are alumina-supported platinum, ruthenium, and rhodium, operating at temperatures between 120 and 160°C. In a mixture of ~1% CO in H_2-rich gas, CO was found to be completely oxidized by addition of an approximately fourfold stoichiometric amount of oxygen ($\lambda \sim 4$), corresponding to an overall process selectivity of ~25% (8–10). The dependence of the CO conversion rate and selectivity as a function of temperature, λ-value, and contact time was examined in detail for alumina-supported platinum metals (6, 11–13) and for Pt supported on zeolite (14). Oh and Sinkevitch (11) observed a selectivity of ~40% for Pt/γ-Al_2O_3 and a much higher selectivity and reactivity of ~80% for the Ru/γ-Al_2O_3 and Rh/γ-Al_2O_3 catalysts at close to 100% CO conversion in an integral flow reactor under non-steady state conditions in H_2-rich gas (0.85% H_2, 900 ppm CO). Studies using more realistic H_2 concentrations arrived at a smaller overall selectivity of ~25% on Ru/γ-Al_2O_3 and Rh/γ-Al_2O_3 (8), or 40–50% for close to 100% CO conversion on Pt/A-Zeolite and Pt/γ-Al_2O_3 (14).

All of the above studies were integral flow measurements which, due to the undefined concentration and temperature gradients in the reactor, do not allow the quantitative determination of the reaction kinetics. Hence, the exact kinetics and the mechanism of the CO oxidation in a H_2 atmosphere are so far unknown. In particular, it is unclear how CO concentration influences the selectivity, which is surprisingly high, considering both the high activity of the platinum metals for hydrogen oxidation (15) and the large partial pressure ratio of p_{H_2}/p_{CO} in the above processes. Inferences on the mechanistic aspects of the selective CO oxidation may be drawn from what is known for the CO oxidation reaction (without hydrogen) on single-crystalline and supported catalysts. In early reviews by Engel and Ertl (16, 17), focusing on the CO oxidation reaction on both single crystals and polycrystalline materials under UHV (ultra high vacuum) conditions, a distinction was made between two reaction regimes: (a) a *high rate branch* where the CO surface concentration is very small, occurring at high temperatures and/or λ-values (*oxidizing conditions*); (b) a *low rate branch* in which the surface is predominantly covered with adsorbed CO, occurring at low temperatures and/or λ-values (*reducing conditions*). For both branches a Langmuir–Hinshelwood mechanism was proposed. The *low rate branch* is associated with a reaction order approaching −1 for p_{CO} and close to +1 for p_{O_2} (CO desorption limited), while the *high rate branch* exhibits a reaction order of +1 for p_{CO} and zero for p_{O_2}. More recent studies dealing with high-pressure CO oxidation on single-crystalline platinum metals and supported Pt-catalysts (18, 19) come to similar conclusions, indicating that the reaction mechanism of CO oxidation under UHV and high pressure conditions are essentially identical (in the absence of mass transport effects). FTIR measurements during CO oxidation on Pt/Al_2O_3 under atmospheric pressures by Haaland and Williams (20) demonstrated that the λ-value at which the transition between the two reaction branches occurs (λ_t) is a function of temperature; it decreases from 16 to 8 to 2 as the reaction temperature is raised from 190 to 220 and finally to 250°C, respectively.

Assuming that the addition of H_2 to the CO/O_2 mixture does not fundamentally alter the CO oxidation mechanism, one would expect the reaction to occur in the *low rate branch*, i.e., on a surface predominantly covered with adsorbed CO (CO_{ads}) at conditions which prevail in the PROX process on Pt/γ-Al_2O_3, i.e., at temperatures below 250°C and $\lambda \leq 2$. Indeed, *in situ* DRIFTS (diffuse reflectance FTIR) measurements on Pt/γ-Al_2O_3 with simulated reformer gas showed that the CO coverage, θ_{CO}, closely corresponds to its saturation value at the reaction temperature (21). The reported high selectivity on platinum (11–14) can easily be rationalized by the blocking action of CO_{ads}, thereby reducing the rate of hydrogen adsorption and oxidation. Since an increase in reaction temperature is concomitant with an increase in the CO desorption rate, the selectivity is expected to decrease with temperature, as was demonstrated for Pt/Al_2O_3 (14). Similarly, a decrease in the CO concentration should decrease its equilibrium surface concentration, again leading to a reduced selectivity.

2. EXPERIMENTAL

2.1. Catalysts and Reactants

Most experiments were conducted with a 0.5 wt% Pt/γ-Al_2O_3 catalyst powder (Degussa, F 213 XR/D) with a support particle size of ~20 μm and ~100 m^2/g BET surface area (Degussa γ-Al_2O_3 type 213). Comparison was made with a 5 wt% Pt/γ-Al_2O_3 powder catalyst from Johnson Matthey (Type 125, #55654), which had the same nominal support particle size and BET surface area. Catalysts and the pure support material were dried at 300°C in air and stored in a desiccator. Prior to the experiments, the catalysts were conditioned by calcination in a 10% O_2/N_2-mixture at 350°C (30 min, 20 nml/min), followed by reduction in H_2 at the same temperature and flow rate. Subsequently, the reactor was cooled down to reaction temperature in H_2. Similar procedures for catalyst conditioning have been reported in the literature and were shown to reproducibly yield clean surfaces (22–24), while the temperature is sufficiently low to prevent the sintering of platinum particles (25). The dispersion, *D*, of conditioned catalysts was estimated by means of CO-adsorption, yielding values of about 38% for the 0.5 wt% Pt/γ-Al_2O_3 catalyst and ~13% for the 0.5 wt% Pt/γ-Al_2O_3 catalyst.

All gases were supplied by Linde AG. The pure gases (H_2 (N5), N_2 (N5, CO-free), and CO (N4.7) in an aluminum cylinder) were further purified with gas filter units

(Chrompack AG) to remove traces of oxygen, water, and hydrocarbons. The gas mixtures, 2% CO (N4.7) in H_2 (N5.0) in an aluminum cylinder and 10% O_2 (N5.0) in N_2 (N5.0, CO-free), were used directly. An additional gas mixture (1% O_2, 1% CO, 1% CO_2, 1% CH_4, 75% H_2, the rest is N_2) was used for calibration. For CO-containing gases both the gas cylinder regulators and the tubings were of either brass or copper to prevent nickel and iron carbonyl formation.

2.2. Reactor System and Analytical Method

Gases were mixed with mass flow controllers (Hastings, HFC-202), calibrated for the above gases and gas mixtures with a soap-bubble flow meter: 20 nml/min for O_2/N_2, 50 nml/min for N_2, and 100 nml/min for both H_2 and CO/H_2 (nml/min evaluated at standard conditions of 0°C and 1.013×10^5 Pa). This way, accurate and reproducible $CO/O_2/H_2/N_2$-mixtures could be created at a flow rate of typically 120 nml/min. The gas mixture could then either be sent through the reactor or directly to the gaschromatograph for analysis. The reactor consisted of a quartz tube (4 mm ID) located in a ceramic tube furnace. The weight of the catalyst bed ranged from ~50–100 mg, which resulted in a length of ~5–10 mm and a nominal space velocity of ~16–32 s^{-1}.

Quantitative analysis of H_2O, CO, CO_2, O_2, and CH_4 in the H_2/N_2 matrix was performed by gaschromatography (Dani, model GC 86.10). Column switching in combination with two-channel detection (thermal conductivity detectors) allowed to separate CO_2 and H_2O from the other gases on a polar column (Hayesep Q, $8' \times 1/8''$, 80–100 mesh), followed by the separation of O_2, N_2, CH_4, and CO on a molecular sieve (molecular sieve 5 Å, $8' \times 1/8''$, 80–100 mesh). Using H_2 as carrier gas (20 nml/min) and an oven temperature of 80°C, the complete analysis required 10 min, yielding a quantification limit (LOQ) of ~10 ppm for CO, CO_2, O_2, and CH_4. Because of the low oven temperature, the concentration of product water could only be assessed with an accuracy of ±20%. For CO-TPD measurements, which were performed in a larger reactor (~2 g of catalyst), helium carrier gas was used (13 nml/min) at an oven temperature of 140°C, resulting in an acquistion time of less than 3 min.

The CO conversion, X_{CO}, was calculated from the CO_2 concentration at the reactor exit. Only if significant amounts of methane could be detected, the conversion was calculated over the CO balance directly. Owing to the merely semiquantitative measurement of the water concentration, the selectivity (Eq. [1]) had to be assessed *via* the oxygen mass balance (CO_2 and H_2O formation):

$$S = \frac{0.5 \times c^{out}_{CO_2}}{c^{in}_{O_2} - c^{out}_{O_2}} = \frac{0.5 \times c^{out}_{CO_2}}{\Delta c_{O_2}}. \qquad [3]$$

At the lowest CO concentration of ~200 ppm, the error for X_{CO} was on the order of ±3% and less than ±0.5% for concentrations ≳1000 ppm. The determination of the selectivity *via* Eq. [3] was less accurate because of the generally small difference in the denominator; the absolute error for the selectivity is approximately ±4% over the entire concentration range.

2.3. Activity Measurements

In all experiments we observed a significant initial deactivation over the first two hours from the time a catalyst was put on-stream (approximately a factor of two). This occurred both with freshly reduced samples, as well as with aged catalysts which had been taken off-stream for several minutes. Any further deactivation was very slow, within less than 5% in an additional 10-h time period. The same phenomenon, was reported for CO oxidation (without H_2) on Pt/SiO_2 and Pt/Al_2O_3 catalysts under similar reaction conditions (22, 23, 26, 27). In subsequent FTIR studies (28, 29) it was concluded that this effect is due to the initial nonequilibrium CO coverage upon exposure of the catalyst to the CO/O_2-reaction mixture. These observations are congruent with our own *in situ* DRIFTS measurements on 0.5% Pt/γ-Al_2O_3 during the selective CO oxidation reaction (21, 30). Therefore, in order to closely represent steady-state conditions, the reaction rates in our differential flow experiments were evaluated from data which were recorded roughly 2 h after the gas concentration at the reactor entrance had been changed. For the more qualitative temperature-ramp experiments in the integral flow mode starting at 75°C, the temperature was increased in 25°C increments every 15 min and a data point was acquired just before advancing to a higher temperature.

The conversion of all reactants in our differential flow measurements was maintained below 5% at CO concentrations on the order of 1% and below ~20% for CO concentrations ≲1000 ppm. By limiting the conversion of both CO and O_2, the isothermicity of the catalyst bed could be guaranteed (<10°C based on the adiabatic temperature rise). Absolute reaction rates were then evaluated for the average concentration of each component $\bar{c}_i$, entering and exiting the reactor (31):

$$r_{CO_{mass}} = \frac{X_{CO}\dot{V}_{tot}c^{in}_{CO}}{m_{Pt}} \quad \text{in } \left[\text{mol}_{CO} \cdot g^{-1}_{Pt} \cdot s^{-1}\right] \qquad [4]$$

with m_{pt} being the mass of platinum in the reactor bed and $\dot{V}_{tot}$ being the total molar flow rate. The accuracy of the measured rate, r_{CO}, is then approximated by the deviation of $\bar{c}_i$ from c^{in}_i, which is on the order of ±10% for a maximum conversion of 20%. Using the catalyst dispersion, the mass-based rates were converted into turnover frequencies (TOF).

On account of the high activity of even the 0.5% Pt/γ-Al_2O_3 catalyst above 150°C, the catalysts had to be diluted

with pure support material in order to maintain sufficiently low conversion levels. The dilution ratio, R_{dil}, specifies the ratio of catalyst mass to the mass of the diluted mixture (1 : 1 meaning undiluted). In a separate experiment with pure γ-Al_2O_3 it was shown that the conversion of both O_2 and CO is well below 0.5% of their total amounts over the entire temperature range investigated in the differential flow mode ($\leq$250°C). At the reaction rates of this study (TOF < 4), mass transport resistances in form of either film diffusion and/or pore diffusion can be excluded (see Ref. (31, p. 498)).

3. RESULTS

3.1. Catalyst Characterization by CO-TPD

The 0.5% Pt/γ-Al_2O_3 catalyst was characterized first by CO-TPD (Fig. 1), recorded after saturation with CO at 25°C. At a linear temperature ramp of 3°C/min, three peaks/shoulders marked A through C can be reproducibly distinguished at 120, 215, and 260°C, respectively. These results can be compared with previous data from either Pt/Al_2O_3 supported catalysts (25, 32, 33) or from planar model surfaces (34–36) and stepped single crystals (37, 38). At the slow temperature ramp in our study, transport resistances are negligible (39) and consequently we find good agreement with other studies, where these conditions are fulfilled, either for porous supports and similarly low heating rates (32), or for planar model catalysts with atomically thin Al_2O_3-films supporting nano-sized platinum particles (34–36). In contrast, at high heating rates with porous catalysts (1–2°C/s), CO desorption takes place over a broad temperature range up to ~600°C (25, 33). For their model system, Altman and Gorte (34, 35) observed a systematic variation of the peak intensity with cluster size; the high temperature peak dominates the spectrum for Pt particle diameters on the order of 1 nm, while the low temperature peak is strongest for particles above ~4 nm diameter. For supported Pt catalysts, the most frequently observed particle morphology is that of a (truncated) cubooctahedron with (100) and (111) crystal planes (40), the features of which are closely resembled by Pt(335) single crystals (37, 38, 41). The close agreement between the desorption peak temperatures/shapes of the Pt(335) surface with those obtained on Al_2O_3-supported catalysts confirms this idea.

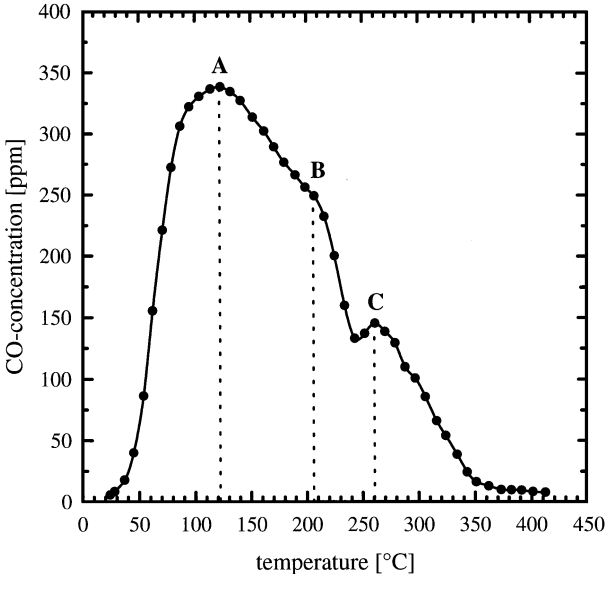

FIG. 1. CO-TPD of 0.5% Pt/γ-Al_2O_3 (2.0 g) at a linear temperature ramp of 3°/min.

The small desorption feature at 260°C (Peak C, Fig. 1) finds no pendant in the CO desorption spectra on model systems under UHV conditions. It could be explained by the decomposition of formate species which are formed by the reaction of CO with support hydroxyl groups (30). Although the contribution from peak C is probably not associated with CO desorption from Pt-sites, the resulting error of ~10–15% in the dispersion is negligible considering other sources of error. Using an adsorption stoichiometry of CO/Pt of 0.7, which was suggested for Pt/γ-Al_2O_3 catalysts (25) (consistent with the CO saturation coverage for low-index faces at 25°C: 0.88 for Pt(110) (42); 0.49 for Pt(111) (43); and 0.77 for Pt(100) (43)), a dispersion of 38% is calculated from Fig. 1 for 0.5% Pt/γ-Al_2O_3. This corresponds to a mean particle size of ~4 nm for spherical or hemispherical geometry. The shape of our CO-TPD spectrum agrees well with the spectrum observed by Altman and Gorte (34) for 5 nm Pt particles.

3.2. Integral Flow Measurements

3.2.1. CO oxidation without H_2. To qualitatively characterize the CO oxidation activity of Pt/γ-Al_2O_3 in the absence of H_2 we measured the conversion of 1% CO to CO_2 over the 0.5% Pt/γ-Al_2O_3 catalyst as a function of temperature for $\lambda = 2$ in pure nitrogen background (solid symbols in Fig. 2). Below 125°C, CO oxidation is very slow with conversions less than 1%. As the temperature is raised, X_{CO} increases first slowly and suddenly picks up at ~175°C, reaching full CO conversion above 225°C. The sudden increase in CO conversion at the *ignition temperature*, which is defined as the temperature of maximum gradient in a plot of X_{CO} *versus* T, is related to the onset of CO desorption (15-17). For an identical gas mixture at comparable space velocities, Anderson (44) observed an *ignition temperature* of ~185°C on 1% Pt/γ-Al_2O_3, which moved towards lower temperatures with increasing λ. Even under UHV conditions on Pt(110), the behavior is almost identical, yielding an *ignition temperature* of ~190°C for $\lambda = 2.6$ (45).

3.2.2. CO oxidation in the presence of H_2. If we add 75% H_2 to the above reaction mixture (Fig. 2, open circles), the *ignition temperature* decreases by about 30°C to ~170°C, as was observed in earlier studies (11, 46).

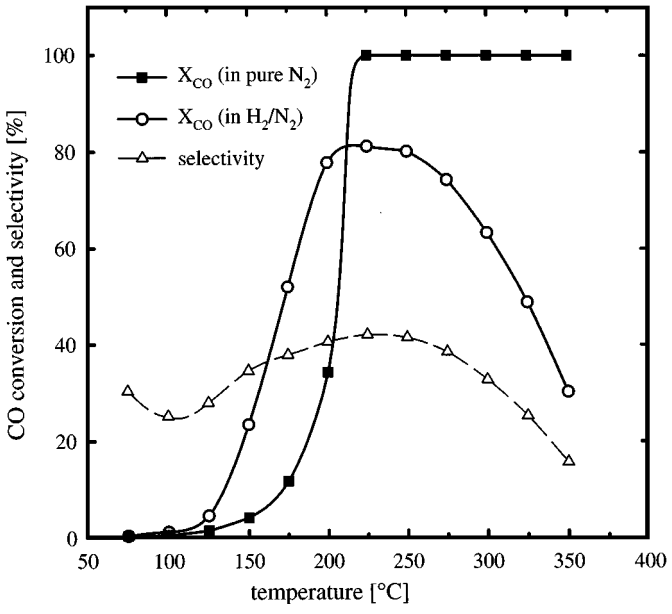

FIG. 2. Variable temperature measurements on 0.5% Pt/γ-Al_2O_3 (100 mg) at $\lambda = 2$. The filled symbols refer to the oxidation of 1% CO in pure N_2, the open symbols show the oxidation of 1% CO in 75% H_2; the rest is N_2. $\dot{V}_{tot} = 120$ nml/min.

At temperatures above 175°C, the oxygen concentration within the catalyst bed drops to zero and oxygen becomes rate-limiting. Therefore, the maximum CO conversion at $\lambda = 2$ is ~80% and more or less contact-time independent. For this reason, it is not surprising that the CO conversion in a similar gas mixture (1% CO, 1% O_2, 98% H_2) over Pt/γ-Al_2O_3 at ≥175°C (14) is the same as in Fig. 2, even though the contact-time ($m_{Pt}/\dot{V}_{tot}$) is 30 times larger. Hence, the CO conversion does **not** reflect the CO reaction rate at high temperatures since it is O_2-limited.

The decrease in CO conversion (to CO_2) above 225°C is again related to the rate-limiting effect of oxygen; at temperatures exceeding 175°C, the amount of O_2 available for CO oxidation is determined by the amount of O_2 consumed for the simultaneously occurring H_2 oxidation reaction. Therefore, the decrease of X_{CO} above ~250°C is a consequence of the loss of selectivity, which decreases continuously above ~250°C to less than 20% at 350°C. These results are in quantitative agreement with the data in Ref. (14). The observed selectivity decrease at ≳250°C for $\lambda = 2$ may be understood on the basis of FTIR results by Haaland and Williams (20); the λ-value for the *low* to *high rate branch* transition in CO oxidation on Pt/γ-Al_2O_3, λ_t, decreases to a value of two as the temperature approaches 250°C from below. For our experiments conducted at $\lambda = 2$ (Fig. 2) this means, that the "protective" CO coverage should decrease above ~250°C (i.e., when $\lambda = \lambda_t$), leading to the observed loss of selectivity at high temperatures. The low-temperature behavior of the selectivity, i.e., its increase with temperature from 100°C to 225°C is more difficult to understand and a tentative model to explain its origin will be advanced in Section 4.1.

3.2.3. Methanation. Generally, platinum is known to be a poor catalyst for methanation reactions if compared to Ni or Ru (15, 18). Nevertheless, it has been shown that the methanation reaction in H_2/CO mixtures, occurring at a very low rate on polycrystalline Pt under atmospheric pressure, can be enhanced if Pt is supported on oxide materials. This support-induced enhancement decreases in the order $TiO_2 > Al_2O_3 > SiO_2$ (47). In the present investigation, the formation of CH_4 can be observed at temperatures exceeding 250°C. At 350°C the CH_4 concentration in the reactor exit stream amounts to 0.02%, corresponding to a CO conversion into CH_4 of $X_{CH_4} \sim 2\%$. Since the overall CO conversion (to CO_2 and CH_4) at this temperature is only ~30%, the methane turnover frequency can be estimated to be $\sim 2 \times 10^{-2}\ s^{-1}$. For comparison, rates at the same temperature in 400 Torr H_2 and 100 Torr CO are $4 \times 10^{-3}\ s^{-1}$ and $8 \times 10^{-2}\ s^{-1}$ for polycrystalline Pt and TiO_x-covered Pt, respectively (48), in good agreement with our results. The reported apparent activation energy for the methanation reaction on polycrystalline platinum (79 kJ/mol (48)) is consistent with the approximately 20-fold lower methane formation rate of $10^{-3} s^{-1}$ observed in our experiments at 250°C and the value of $3 \times 10^{-3}\ s^{-1}$ on Pt/Al_2O_3 reported at 270°C (26). As will be shown later (Section 3.3), the turnover frequencies for CO oxidation at 250°C are on the order of $10^0\ s^{-1}$ (Fig. 4a), so that the rate of methanation in the envisaged temperature range (~150–250°C) is some three orders of magnitude lower than the CO oxidation rate. Therefore, CO methanation is expected to be insignificant for PROX on Pt/γ-Al_2O_3 catalysts.

3.2.4. Comparison of different Pt/γ-Al_2O_3 catalysts. In order to examine whether activity, selectivity, and methanation of Pt/γ-Al_2O_3 catalysts depend on catalyst loading and Pt particle size, d_{Pt}, we compared the performance of the 0.5% Pt/γ-Al_2O_3 catalyst ($D \sim 38\%$, $d_{Pt} \sim 4$ nm) discussed before with that of a 5% Pt/γ-Al_2O_3 catalyst ($D \sim 13\%$, $d_{Pt} \sim 12$ nm). The dependence of the selectivity with temperature and the onset of CH_4 formation are the same for both catalysts. The reduction of the *ignition temperature* for the high-loading catalyst to ~120°C, compared to ~170°C for the low-loading catalyst can be understood from the larger contact-time ($m_{Pt}/\dot{V}_{tot}$) for the former catalyst, *viz.*, $2.3 \times 10^{-3}\ g_{Pt} \cdot s \cdot cm^{-3}$ *versus* $2.5 \times 10^{-4}\ g_{Pt} \cdot s \cdot cm^{-3}$. The value of $m_{Pt}/\dot{V}_{tot}$ in the study by Oh and Sinkevitch (11) ($2 \times 10^{-3}\ g_{Pt} \cdot s \cdot cm^{-3}$) is similar to our experiment with 5% Pt/γ-Al_2O_3, producing an identical *ignition temperature* of ~140°C.

3.3. Differential Flow Measurements

The standard method for the determination of reaction orders is to vary the partial pressure of one of the reactants,

while keeping all other reactants constant. In the present study, however, this approach was not followed, since it would entail measurements over a large range of λ-values, which is undesirable for two reasons: (a) prime criterion for the selective CO oxidation is the minimization of hydrogen oxidation at complete CO oxidation so that the relevant range of λ-values is limited (λ ∼ 1–4); (b) a large variation of λ, in particular to high values, may lead to a transition between different reaction regimes (*low* to *high rate branch*) which would invalidate the experimental approach because of a change in mechanism. Therefore, the CO concentration dependence of selectivity and reactivity was investigated by changing the CO concentration **at constant** λ rather than at constant O_2 concentration.

3.3.1. Selectivity and rate versus temperature. Figure 3a shows the variation of the CO oxidation rate (in TOF) as a function of CO partial pressure **at constant** λ in simulated reformer gas (0.02–1.5% CO, 75% H_2, the rest is N_2).

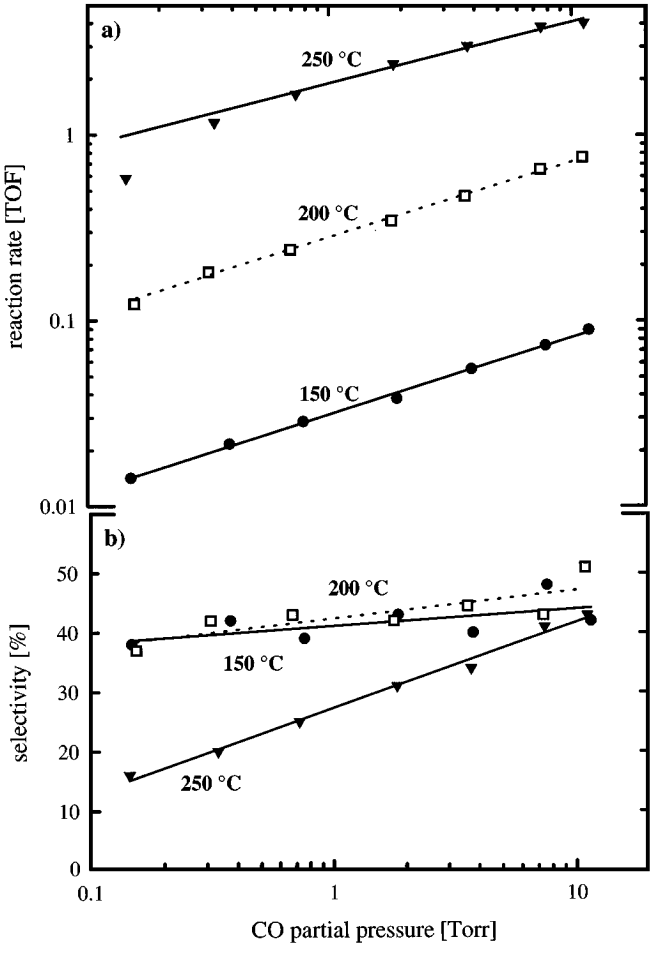

FIG. 3. CO concentration dependence at λ = 2 of (a) turnover frequency and (b) selectivity: ● = 150°C; □ = 200°C; ▼ = 250°C; R_{dil} was 1 : 3 (150°C), 1 : 9 (200°C), and 1 : 90 (250°C). Simulated reformer gas (75% H_2; the rest is N_2); $\dot{V}_{tot}$ = 120 nml/min; catalyst bed weight 75 mg.

The CO oxidation rate exhibits a weak dependence on the CO partial pressure at λ = 2, indicated by the least-squares regression lines with a slope of ∼0.4 (its meaning will be discussed in Section 4.2). As the temperature is increased, the reaction rates increase by a factor of about 10 for every 50°C, but the behavior of r_{CO} *versus* p_{CO} does not change, indicating that the reaction mechanism remains the same (the deviation at 250°C and low p_{CO} is due to a too large O_2 conversion which violates the differential flow requirement).

The corresponding selectivities are shwon in Fig. 3b. At 150 and 200°C, the selectivity is essentially independent of the CO partial pressure, with only a minor decrease of ∼5% with decreasing CO pressure over close to two orders of magnitude in CO concentration (0.02–1.5%). The absolute values of ∼40–45% compare well with what was observed in Fig. 2. Even though the scatter in the selectivity data is higher than in the rates, they clearly display a maximum at 200°C, consistent with the shape of the selectivity *versus* temperature curve in the integral flow measurements. At 250°C, however, a definite decrease in selectivity with decreasing CO partial pressure can be observed, reaching ∼15% at a CO concentration of ∼200 ppm. It is related to the decrease in CO readsorption rate, $r_{CO,\,ads}$, with diminishing p_{CO} (see Section 4.1), which eventually reduces the CO coverage to the very small values inferred from CO-TPD at 250°C (Fig. 1). This behavior is not apparent in the integral flow data (Fig. 2) since the lowest CO concentration (i.e., at the reactor exit) at 250°C is still as large as ∼0.2%, corresponding to a mean CO concentration over the reactor bed of $\bar{c}_{CO} \sim 0.6\%$ (∼4.5 Torr). Therefore, to a zero order approximation, the observed *integral* selectivity (Fig. 2) should be similar to the value of the *differential* selectivity at $\bar{c}_{CO}$ in the integral reactor. This indeed can be confirmed in the following example: at 250°C the *integral* selectivity is ∼40% and $\bar{c}_{CO}$ is about 0.6% (Fig. 2), a concentration at which the *differential* selectivity shown in Fig. 4b is ∼38% (Fig. 3b).

The apparent activation energy for the data in Fig. 3, spanning a CO concentration range from ∼0.05–1% CO (0.38–7.6 Torr) at λ = 2 yields a value of 74 ± 2 kJ/mol. Comparing this with published apparent activation energies on supported Pt catalysts and Pt single crystals under high pressure conditions for the oxidation of CO in the absence of H_2, we find excellent agreement with measurements conducted in the same temperature range on Pt/γ-Al_2O_3 and Pt/SiO_2, with values between 67 and 80 kJ/mol (23, 26) (Table 1). Further examination of Table 1 also reveals the general trend toward lower apparent activation energies at temperatures $\lesssim$170°C (56–65 kJ/mol (26, 49, 50)) and toward higher values at temperatures $\gtrsim$230°C (125 and 138 kJ/mol (18, 51)) in the case of both supported catalysts (26) and single crystals (18). Generally, the occurrence of activation energies above 100 kJ/mol is thought to be related to a change in reaction mechanism at high

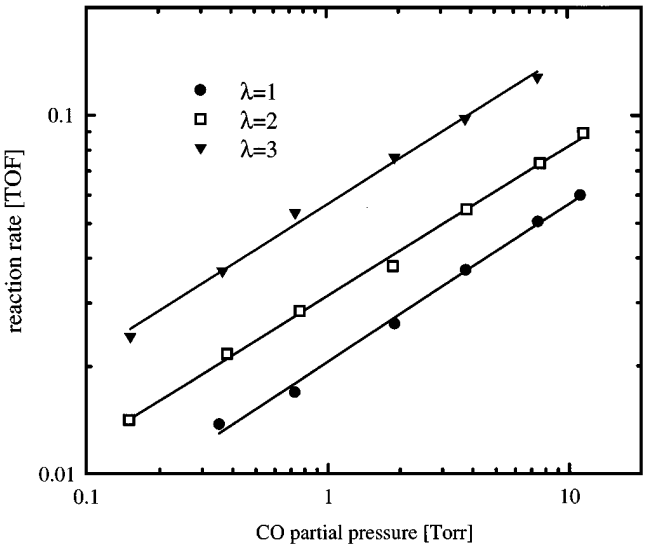

FIG. 4. CO concentration dependence at constant λ and at 150°C (75% H_2; the rest is N_2): λ = 1 (●); λ = 2 (□); λ = 3 (▼). Catalyst bed weight and R_{dil}: 50 mg and 1 : 1 (λ = 1); 75 mg and 1 : 3 (λ = 2); 50 mg and 1 : 3 (λ = 3). $\dot{V}_{tot}$ = 120 nml/min.

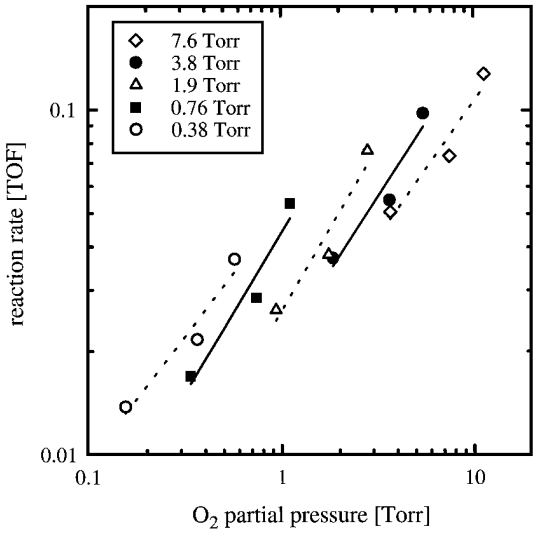

FIG. 5. Double-logarithmic plot of r_{CO} *versus* p_{CO} based on the data shown in Fig. 4. 150°C in simulated reformer gas (75% H_2; the rest is N_2).

temperatures (18). The exceptionally low activation energy reported by Muraki *et al.* (52) probably results from the fact that it was not evaluated at *steady state*. What is interesting, however, is that the addition of water vapor decreases the activation energy (Table 1), a point to which we will return in Section 4.3.

3.3.2. Selectivity and rate versus λ. As a next point we investigated the effect of λ on both reaction rate and selectivity in simulated reformer gas at a temperature of 150° C. Figure 4 shows that the increase of the reaction rate with p_{CO} at constant λ (λ = 1 and 3) is the same as was observed for λ = 2 in Fig. 3 with a reaction order with respect to p_{CO} of ~0.4 **at constant** λ. As would be expected, the reaction rate at constant p_{CO} increases with λ, i.e., with oxygen partial pressure. Even though the oxygen partial pressure range is limited, cross-plotting the data in Fig. 3 may serve as an estimate of the reaction order with respect to p_{O_2} (Fig 5). For CO concentrations ranging from ~500 ppm to 1%, the oxygen reaction order determined from Fig. 5 is $\alpha_{O_2} = +0.8$ with a random (p_{CO}-independent) variation of ±13%. This is in good agreement with literature data for supported and single-crystalline platinum under high pressure conditions (Table 1), where the CO oxidation reaction (in the absence of H_2) in the *low rate branch* is characterized by $\alpha_{O_2} \sim +1$. The fact that the selectivity at 150°C is practically independent of λ implies that the rate of both H_2 and CO oxidation have the same dependency on the oxygen partial pressure, an issue to which we will return in Section 4.1.

3.3.3. The effect of H_2 on CO oxidation. As discussed in Section 3.2.2, the presence of H_2 in a CO/O_2-mixture

TABLE 1

Apparent Activation Energies and Reaction Orders with Respect to p_{O_2} (α_{O_2}) and p_{CO} (α_{CO}) for the CO Oxidation on Supported and Single-Crystalline Platinum at Atmospheric Pressure

System	Reaction conditions	*T*-range	E_A [kJ/mol]	α_{O_2}	α_{CO}	Reference
$Pt/\gamma\text{-}Al_2O_3$	0.38–7.6 Torr CO; λ = 2; 75% H_2	150–250°C	72–76	+0.8	−0.4	This work
$Pt/\gamma\text{-}Al_2O_3$	7.6 Torr CO, λ = 1	<200°C	55	+1	−1.5	Muraki *et al.* (52)
	7.6 Torr CO, λ = 1; 20 Torr H_2O		45	+1	−0.7	
$Pt/\gamma\text{-}Al_2O_3$	23 Torr CO, λ = 1	100–220°C	67–71	+0.7	−0.1	Sarkany and Gonzales (23)
Pt/SiO_2	10 Torr CO, λ = 1	<150°C	56	+0.9	−0.2	Cant *et al.* (26)
		~200°C	≈80			
Pt/SiO_2	15 Torr CO, λ = 0.8	~180°C	72–80	+1	<0	Cant (22)
$Pt/\alpha\text{-}Al_2O_3\{0001\}$	10 Torr CO, λ = 2	>280°C	125	+1	−1	Zafiris and Gorte (51)
Pt(111)	5 Torr CO, λ = 2	<160	65	—	—	Hardacre *et al.* (49)
Pt(100)	8 Torr CO, λ = 1	<170°C	56	+1	0 to −0.6	Berlowitz *et al.* (50)
		>230°C	138	+1	−0.9	Rodriguez and Goodman (18)

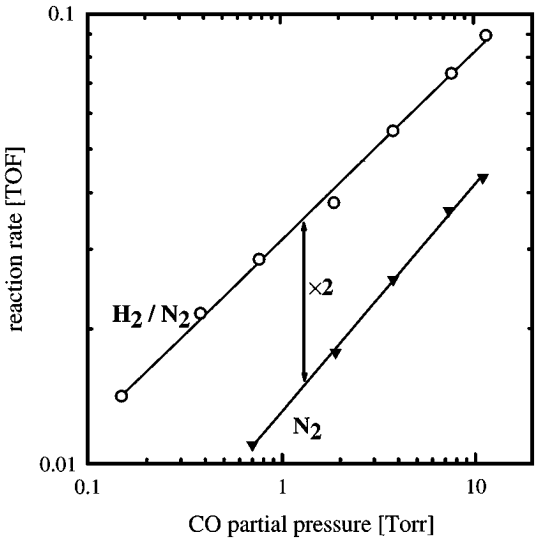

FIG. 6. CO oxidation rates (TOF) on Pt/γ-Al_2O_3 at 150°C as a function of p_{CO} at $\lambda = 2$ in: (◯) simulated reformer gas (75% H_2; the rest is N_2); (▼) pure N_2 background. $\dot{V}_{tot} = 120$ nml/min.

reduces the *ignition temperature* by ∼30°C, which is equivalent to a roughly fivefold rate enhancement in the variable-temperature experiment shown in Fig. 2. To quantify the H_2-induced rate enhancement, we conducted experiments on the same catalyst (0.5% Pt/γ-Al_2O_3) at 150°C and $\lambda = 2$ with and without H_2 background, shown in Fig. 6. While the variation of $\log(r_{CO})$ with $\log(p_{CO})$, i.e., the slopes of the lines in Fig. 6, does not change very much by the addition of hydrogen, the reaction rate in the presence of H_2 at 150°C is about a factor of 2 larger in comparison to the reaction in pure N_2 background. The same behavior was described by Muraki *et al.* (52) for CO oxidation on Pt/γ-Al_2O_3, where the reaction rate at 150°C increased by a factor of ∼3 upon the addition of ∼2 Torr H_2 to 7.6 Torr CO ($\lambda = 0.9$). A similar enhancement of r_{CO} was produced by adding ∼20 Torr of water vapor to the above CO/O_2 mixture. This effect of water on r_{CO} was qualitatively reproduced in our laboratory.

4. DISCUSSION

In the following, we will discuss in more detail the selectivity of the CO oxidation in simulated reformer gas, focusing on the behavior of the selectivity at low temperatures and at its decrease at high temperature in conjunction with low CO partial pressures. Since the relevant range of λ-values for the PROX process is very narrow (see Section 3.3), the change of reaction rate with p_{CO} was measured at constant λ rather than at constant p_{O_2}. For this reason, the reaction order with respect to CO cannot be determined directly. It will, however, be shown that it can be deduced from the measured data by means of a numerical fit of the r_{CO} data to a kinetic rate expression. This will provide an accurate method for data interpolation and will, in turn, allow the comparison between the reaction rates measured in our study and literature data. Finally, we will discuss the observed H_2- and H_2O-induced CO oxidation rate enhancement.

4.1. Selectivity

We will divide the discussion of the selectivity into two parts, focusing on: (i) the temperature region between 150 to 200°C where the selectivity is independent of p_{CO} but increases slightly with temperature, and (ii) the dependence of the selectivity on p_{CO} at 250°C.

4.1.1. Selectivity at 150 and 200°C. To understand the observation that the selectivity of the CO oxidation reaction on Pt/γ-Al_2O_3 is independent of p_{CO} between 150 to 200°C it is helpful to remember that the reaction proceeds in the *low rate branch* (indicated by α_{O_2} being close to +1). For CO oxidation on Pt/Al_2O_3 at atmospheric pressures (without H_2), a saturated monolayer of CO was observed up to ∼220°C for $\lambda \leq 8$ (20). Likewise, our own *in situ* DRIFTS data confirmed full CO coverage in simulated reformer gas (1% CO, $\lambda = 2$, 75% H_2, the rest is N_2) for temperatures $\lesssim$200°C (21). Therefore, the high selectivity in this temperature range is mostly due to the blocking action of adsorbed CO, preventing the oxidation of hydrogen; at 250°C and above (Fig. 2), the selectivity decreases due to CO desorption. The latter effect may be visualized by the CO-TPD spectrum in Fig. 1, demonstrating that only ∼10% of the inital CO coverage remain on the surface at 250°C if it is in equilibrium with ∼150 ppm of CO.

To understand the interrelation between selectivity and the partial pressures of both O_2 and CO, let us rewrite the definition of the selectivity (Eq. [1]) in terms of reaction rates:

$$S = \frac{r_{CO}}{r_{CO} + r_{H_2}} = \frac{1}{1 + r_{H_2}/r_{CO}} \qquad [5]$$

with r_{CO} being the measured CO turnover frequency and r_{H_2} the H_2 oxidation rate. At 150°C and a CO concentration of ∼0.02% ($\lambda = 2$), r_{CO} is two orders of magnitude lower than at 200°C and a CO concentration of ∼1.5% ($\lambda = 2$; see Fig. 3), but the selectivity at both extremes of r_{CO} is essentially identical (∼40%). The same can be observed in Fig. 4, where r_{CO} at 150°C varies by a factor of 10 as both CO and O_2 concentrations are changed, while the selectivity remains at a constant ∼40%. Thus, according to Eq. [5], r_{H_2}/r_{CO} is constant over a large range of concentrations and temperatures; i.e., r_{H_2} is directly proportional to r_{CO} under these conditions. The fact is that CO oxidation in the *low rate branch* is CO desorption limited implies that its reaction rate is limited by oxygen adsorption/dissociation (16, 53). If this is the case, it is clear that the oxidation rate of co-adsorbed hydrogen (54–56) is limited by the same

mechanism, with the consequence that r_{H_2} and r_{CO} are coupled.

In explaining the coupling of r_{H_2} and r_{CO}, we assumed that H_2 and CO are co-adsorbed on the surface so that r_{H_2}/r_{CO} at constant temperature (i.e., the selectivity) should only depend on θ_H/θ_{CO}. Since the selectivity is constant over a wide range of CO concentrations, this implies that θ_H/θ_{CO} must also remain constant which seems reasonable if θ_{CO} is close to saturation. On this premise, we can now hypothesize on the slight increase in selectivity for increasing the temperature from 150 to 200°C (Figs. 2 and 3). The lower adsorption energy of hydrogen (~80 kJ/mol on Pt(111) (57)) compared to CO (~140 kJ/mol on Pt(111) (58, 59)), leads to a reduction of the (small) hydrogen coverage with increasing temperature, while θ_{CO} remains close to saturation. This leads to a decrease in θ_H/θ_{CO} which is equivalent with a decrease in r_{H_2}/r_{CO}, and hence, an increase of the selectivity (Eq. [5]).

4.1.2. Selectivity versus p_{CO} at 250°C. At 250°C, the selectivity at p_{CO} above 10 Torr (Fig. 3) is almost identical with the selectivity measured at 150°C. If, however, the CO partial pressure is decreased, the selectivity at 250°C falls off significantly, eventually reaching a value of ~15% at ~0.15 Torr CO. This behavior at 250°C implies that the CO coverage must drop from close to saturation at ~10 Torr CO to significantly below saturation at ~0.15 Torr. Assuming first-order Langmuir adsorption and desorption kinetics, the relative CO *equilibrium* coverage at any pressure p_2 ($\theta_{(p_2)}$) (at constant temperature) can be determined if θ_{CO} at pressure p_1 ($\theta_{(p_1)}$) is known:

$$\theta_{(p_2)} = \frac{\theta_{(p_1)}}{\frac{p_1}{p_2}\cdot\left(1-\theta_{(p_1)}\right)+\theta_{(p_1)}}. \qquad [6]$$

In the derivation of Eq. [6], it was assumed that the rate or reaction is negligible, compared to the rate of CO readsorption, which is a reasonable assumption as long as the CO concentration is still in the ppm range.

On the basis of the CO-TPD spectrum in Fig. 1, the relative CO coverage at 250°C is on the order of $\theta_{(p_1)} \sim 0.1$ at a CO pressure $p_1 \sim 150$ ppm (~0.11 Torr). Using these values, we can now calculate the variation of θ_{CO} as a function of CO partial pressure using Eq. [6]. This is shown in Fig. 7. It is apparent, that the relative CO coverage under these assumptions changes from ~0.15 at 0.2 Torr CO to ~0.9 at 10 Torr CO, indicating that the relative CO coverage at 250°C increases from very low θ_{CO} at low CO pressures, to almost saturation coverage at the upper CO pressure in our measurements (i.e., 1.5% CO). Within the framework of the above model, the CO coverage at 250°C in the presence of 10 Torr CO is expected to closely approach saturation due to a high rate of CO readsorption. The absolute values of θ_{CO} in Fig. 7 must be considered with caution, owing to the above simplifications in the model and the fact that the

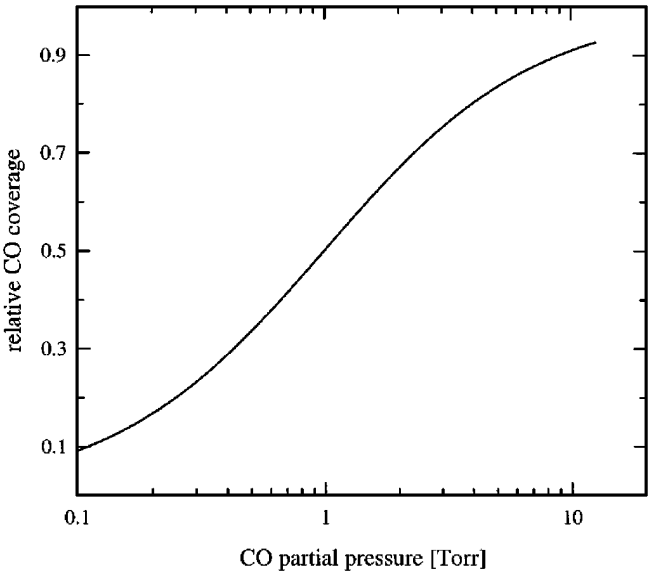

FIG. 7. Evaluation of the relative CO surface coverage at 250°C as a function of CO partial pressure, based on Eq. [6] (see text).

CO concentration measured in the TPD-spectrum (Fig. 1) is an average value over the length of the catalyst bed. Nevertheless, the general variation of θ_{CO} with p_{CO} should be approximated fairly well in Fig. 7 and is consistent with the p_{CO}-dependence of the selectivity at 250°C (Fig. 3), where a high selectivity of ~40% is found at ~10 Torr which then drops to ~15% at ~0.15 Torr.

4.2. Kinetic Model and Comparison with Literature TOF-Data

In Section 3 we evaluated the apparent activation energy ($E_A \sim 74$ kJ/mol) and the reaction order with respect to oxygen partial pressure ($\alpha_{O_2} \sim 0.8$). As discussed, the reaction order with respect to CO, α_{CO}, was not determined directly by variation of p_{CO} at constant p_{O_2}, but it can be estimated from a kinetic model. The rate expression most commonly applied to the CO oxidation reaction is a simple power-law functionality:

$$\ln(r_{CO}) = \ln(k_{CO}) - \frac{E_A}{R\cdot T} + \alpha_{CO}\cdot\ln(p_{CO}) + \alpha_{O_2}\cdot\ln(p_{O_2}). \qquad [7]$$

The experiments in Figs. 3 and 4 were conducted by varying the CO partial pressure while maintaining λ constant, so that under consideration of the definition of λ (Eq. [2]) the slopes of $\log(r_{CO})$ *versus* $\log(r_{CO})$ correspond to

$$\left(\frac{\partial\log(r_{CO})}{\partial\log(p_{CO})}\right)_{\lambda=\text{const}} = \alpha_{CO} + \alpha_{O_2} = \alpha_{CO}^{\lambda}, \qquad [8]$$

where α_{CO}^{λ} is the reaction order with respect to p_{CO} at **constant** λ. Combining $\alpha_{CO}^{\lambda} \approx 0.4$ (from Figs. 3 and 4) with $\alpha_{O_2} \sim 0.8$ (Fig. 5), the reaction order with respect to p_{CO}

TABLE 2

Comparison between Literature Data for CO Oxidation Rates, r_{exp}, in the Absence of H_2 on Supported and Single-Crystalline Platinum at Atmospheric Pressures with Rates Measured in this Work (in the Presence of H_2), r_{calc}, Interpolated by Means of the Parameters in Section 4.2

System	Reference	p_{CO} [Torr]	p_{O_2} [Torr]	λ	Temp.	r_{exp} [s^{-1}]	r_{calc} [s^{-1}]	r_{calc}/r_{exp}
Pt/γ-Al_2O_3 ($D=46\%$)	Muraki *et al.* (52)	7.6	3.3	0.9	150°C	1.1×10^{-2}	4.2×10^{-2}	~3.5
Pt/SiO_2 ($D=22\%$)	Cant *et al.* (26)	9.9	4.9	1	177°C	4×10^{-2}	1.8×10^{-1}	~4
Pt/SiO_2 ($D=6$–81%)	Cant (22, 27)	15.2	6.1	0.8	177°C	1.3–1.5×10^{-2}	1.7×10^{-1}	~10
Pt/α-Al_2O_3{0001} (14 nm)	Zafiris and Gorte (51)	10	10	2	289°C	2.3	13.8	6
Pt(111)	Hardacre *et al.* (49)	6.6	3.3	1	157°C	3×10^{-2}	6.2×10^{-2}	~2
Pt(100)	Berlowitz *et al.* (50)	16	8	1	150°C	1.5×10^{-2}	6.3×10^{-2}	~4
Pt(100)	Rodriguez and Goodman (18)	6	3	1	227°C	1.5×10^{-1}	9.7×10^{-1}	~6

Note. Experimental conditions for the literature data and metal dispersion, D, for supported catalysts are listed below. Rates are in units of TOF.

based on Eq. [8] is $\alpha_{CO}\sim-0.4$. This is in reasonable agreement with the data in Table 1 and further suggests that the selective CO oxidation at our conditions proceeds in the *low rate branch*.

A more precise evaluation of the kinetic parameters is a comprehensive numerical fit of Eq. [7] to all experimental data with initial parameter estimates based on the above values of E_A, α_{CO}, and α_{O_2}. In the following least-squares fit, care was taken to exclude data points for which the average partial pressure of one of the components, $\bar{p}_i$, deviated by more than ±15% from the respective inlet/outlet concentration. This applied to the measurements at the lowest two p_{CO}-values at 250°C and the lowest value at 200°C (Fig. 3). The resulting least-squares parameters (30 data points) are: $k_{CO}=2.23\times10^7\pm1.6\%$ (for pressures in units of Torr and rates in TOF), $E_A=71.1$ kJ/mol ± 1.4%, α_{CO} $-0.42\pm13\%$, and $\alpha_{O_2}=0.82\pm6.5\%$. The maximum deviation between measured and calculated rates of ±15% is consistent with the maximum allowed uncertainty in the reactant partial pressures, $\bar{p}_i$. A comparison of the above parameters with their initial estimates based on data subsets indicates that the entire data set is well represented by Eq. [7].

Literature data on the CO oxidation rate, r_{exp}, under atmospheric pressures in the absence of H_2 are listed in Table 2. Equation [7], in conjunction with the above fitting parameters, was employed to interpolate the oxidation rates measured in our work in the presence of H_2, r_{calc}, in order to facilitate a quantitative comparison over the applicable range of temperatures and pressures. It is quite obvious, that the oxidation rates inferred from our measurements in the presence of H_2 are always larger than the rates reported for the oxidation of CO without H_2 background, with r_{calc}/r_{exp} ranging between ~2–4 at 150°C and ~4–10 at higher temperatures for both single crystals and supported catalysts with widely varying dispersions. At 150°C most of this difference can be accounted for by considering the H_2-induced enhancement of r_{CO} by a factor of ~2 (Section 3.3.3).

4.3. The Effect of H_2 on CO Oxidation

The physical origin of the H_2/H_2O-induced increase in CO oxidation rate has not been explained in the literature so far. UHV studies on Pt(335) have shown that the coadsorption of CO and H_2 produces mixed CO/H islands with CO adsorbed primarily in bridge positions (55, 56), whereas on Pt(112) repulsive CO–H interaction leads to separated islands (54). None of these studies, however, find a H_2-induced desorption of CO which was reported for Pt(111) at low temperatures (60). The latter would, at least qualitatively, explain the observed rate enhancement if we assume that the CO oxidation rate is CO desorption limited. In our *in situ* DRIFTS measurements, however, we did not find a significant decrease in the CO coverage in the presence of H_2 (21), although it cannot be excluded that very small changes in θ_{CO} might produce a large effect on r_{CO}.

A different explanation may be the interaction between the hydroxylated Al_2O_3-support and CO adsorbed on Pt. By this process, formate species are formed on the support, if the CO oxidation reaction is carried out in the presence of either H_2 or H_2O (30). Since the formation of formate species on the Al_2O_3-support consumes Pt-bonded CO, it is conceivable that free Pt-sites for O_2 adsorption/dissociation are produced by this process, thereby effecting an increase in r_{CO}. This would explain the rate enhancing effect of both H_2 and H_2O. It in turn would imply that the effect of H_2 or H_2O on the CO oxidation rate should depend on the support material, an issue which is currently under investigation.

5. PERFORMANCE PREDICTION IN A PLUG FLOW REACTOR

At the end of our study, we will demonstrate the utility of differential flow data for the prediction of the performance of a *plug flow* reactor for CO conversion. At 150°C, the selectivity of the CO oxidation reaction is ~40% for the

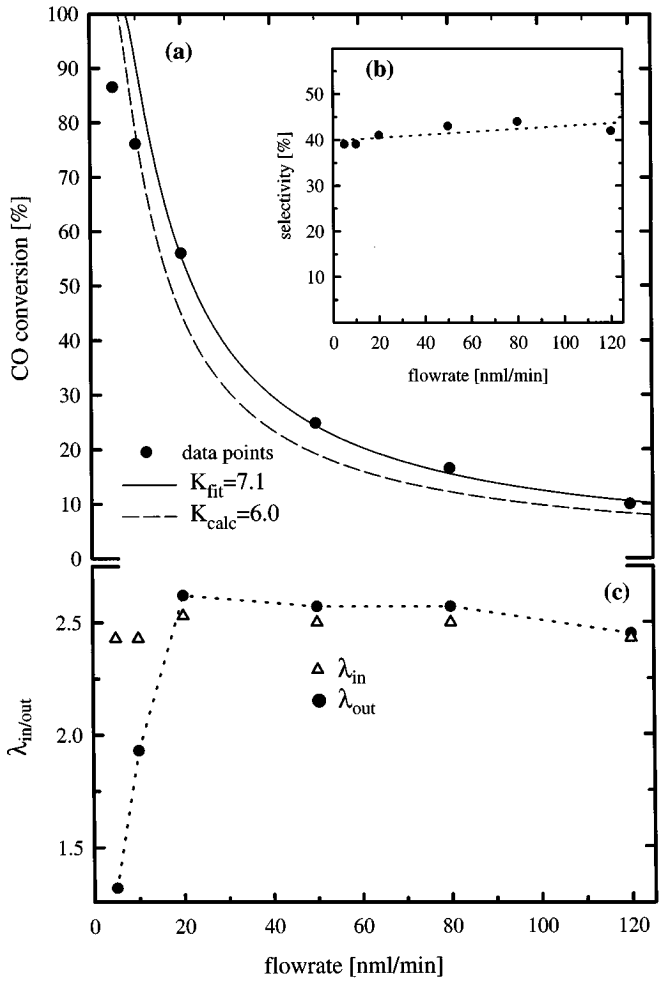

FIG. 8. (a) CO conversion and (b) selectivity as a function of flow rate at a composition of 1% CO, 1.25% O_2 ($\lambda = 2.5$), 75% H_2, the rest is N_2 at 150°C. (c) Actual measurement of the λ-values at the reactor entrance ($\triangle = \lambda_{in}$) and at the reactor exit ($\bullet = \lambda_{out}$). The solid line in (a) is a fit of the CO conversion data to Eq. [10]; the dashed line is based on the calculated K-value of 6.0 nml/min (see text). 75 mg of undiluted 0.5% Pt/γ-Al_2O_3.

entire CO concentration range (Fig. 6b), which implies that a λ-value of 2.5 should suffice to completely oxidize CO. This will be verified in the following experiment, where a gas stream containing 1% CO and 1.25% O_2 ($\lambda = 2.5$) in a 75% H_2/25% N_2 background is passed over the catalyst bed (0.5% Pt/γ-Al_2O_3) at variable flow rate, $\dot{V}_{tot}$. Figure 8 shows the steady-state conversion of CO as a function $\dot{V}_{tot}$, which is inversely related to the contact-time. At the highest flow rate, the conversion is ∼10% and the selectivity is slightly above 40% as expected (Fig. 8b). Consequently, the λ-value at the reactor entrance, λ_{in}, is identical with the value at the reactor exit, λ_{out}. As the flow rate is being decreased to 20 nml/min, the CO conversion increases to ∼55% while the selectivity remains above ∼40% (therefore, λ_{in} equals λ_{out}). Further decreasing the flow rate to 10 and 5 nml/min produces conversions of ∼75 and ∼85%. At this point the selectivity drops slightly below 40% due to the reduced CO partial pressure in the reactor, effecting a decrease of λ_{out}. Thus, the differential flow data can be used to estimate the amount of O_2 required for the selective oxidation of CO (at a given T and λ).

The kinetic expression in Eq. [7] can be applied to calculate the conversion of CO as a function of flow rate. For this purpose, Eqs. [2] and [7] in conjunction with the reaction orders evaluated in Section 4.2 can be rewritten as

$$r_{CO} = k_{CO}/2^{0.82} \cdot e^{-E_A/RT} \cdot p_{CO}^{0.4} \cdot \lambda^{0.82} = k_1 \cdot p_{CO}^{0.4} \cdot \lambda^{0.82}. \quad [9]$$

For the above plug flow experiment (Fig. 8), the relation between $\dot{V}_{tot}$ and X_{CO} can be calculated by combining Eq. [9] with the mass balance over a plug flow reactor. For constant λ and T one attains

$$X_{CO} = 1 - \left(1 - \frac{k_1 \cdot k_2}{\dot{V}_{tot}}\right)^{1.66} = 1 - \left(1 - \frac{K}{\dot{V}_{tot}}\right)^{1.66}, \quad [10]$$

where k_1 is the temperature-dependent rate constant (Eq. [9]) and k_2 is a constant incorporating the CO concentration at the reactor entrance, c_{CO}^{in}, the absolute system pressure, P (in Torr), the λ-value, and other catalyst-related parameters:

$$k_2 = \frac{m_{Pt} \cdot D}{M_{Pt}} \cdot \frac{0.6 \cdot P^{0.4}}{\left(c_{CO}^{in}\right)^{0.6}} \cdot \lambda^{0.82}. \quad [11]$$

For the experimental data in Fig. 8, taken at $P = 760$ Torr, an average λ of 2.55 (see Fig. 8c), a CO concentration of $c_{CO}^{in} = 1\%$, and a catalyst weight of 75 mg, the product of k_1 and k_2 at 150°C equates to $K = 4.44 \times 10^{-6}$ mol/s = 6.0 nml/min. In the range, where λ remains roughly constant over the length of the reactor (the data between 20–120 nml/min), a numerical fit of the conversion *versus* flow rate according to Eq. [10] (solid line in Fig. 8a) yields a value of $K = 7.1$ nml/min. The difference of ∼15% merely reflects our estimated error in the measurement of absolute reaction rates (Section 4.2) and consequently in the evaluation of k_1, so that the agreement between the calculated (dashed line in Fig. 8a) and the fitted lines is quite reasonable. Therefore, the kinetic expression and parameters derived in Section 4.2, provide a satisfactory description of the process kinetics under the conditions of our study. At flow rates of 10 and 5 nml/min, λ is not any more constant over the length of the reactor, thereby invalidating the basic assumption underlying Eq. [10]. Furthermore, as the average value of λ decreases below 2.5 for flow rates below 20 nml/min, the reaction rate decreases accordingly (Eq. [9]), producing a CO conversion which is lower than would be expected, an effect which can be observed in Fig. 8a. Overall, the kinetic expression derived from the differential flow measurements discussed above provides a good basis for the engineering design of a PROX reactor within a temperature range of 150–250°C and λ-values between 1 and 3.

6. CONCLUSIONS

We have shown that the kinetics of the selective CO oxidation on Pt/γ-Al_2O_3 in simulated reformer gas (75% H_2; the rest is N_2) over a wide range of CO concentrations (0.02–1.5%) and PROX-relevant λ-values ($\lambda = 1$–3) can be expressed by a simple power-law rate equation with an Arrhenius term. The reaction orders with respect of p_{CO} (-0.4) and p_{O_2} ($+0.8$) and the apparent activation energy of 71 kJ/mol are consistent with the reaction occuring in the *low-rate* branch, i.e., on a surface predominantly covered by adsorbed CO. Thus, the blocking action of adsorbed CO with respect to oxygen adsorption/dissociation (i.e., oxygen adsorption is rate-limiting) is responsible for the high selectivity of about 40% and the experimental observation that it is independent of the CO partial pressure at 150 and 200°C. The loss of selectivity at 250°C and low CO concentrations (e.g., $S \sim 15\%$ at 0.02% CO) or at temperatures significantly above 250°C can be rationalized by the onset of CO desorption and the concomitant increase in the H_2 oxidation rate.

CO methanation rates on Pt/γ-Al_2O_3 are negligible in the PROX-relevant temperature range between 150 and 250°C. At these temperatures, methanation activities and selectivities were essentially identical on high- (5%) and low-loading (0.5%) Pt/γ-Al_2O_3 catalysts. Both integral and differential flow measurements revealed a CO oxidation rate enhancement by a factor of approximately two in the presence of hydrogen. This effect may be due to H_2-induced CO desorption or to the interaction of the hydroxylated Al_2O_3-support with CO adsorbed on Pt. It will be subject to further investigations.

Finally, the deduced kinetic rate equation was tested by mathematically modeling the CO conversion in a plug-flow experiment with variable flow rate (i.e., variable contact time). Measured CO conversions were in quantitative agreement with the CO conversions predicted by our kinetic model. The optimum temperature for the PROX process on Pt/γ-Al_2O_3 catalysts ~200°C, yielding a combination of high reaction rates and high selectivity.

ACKNOWLEDGMENTS

We thank Thomas Häring for his help in building the reactor, Albrecht Rämisch for the preparation of the quartz tubes, and Dr. E. Auer from Degussa for providing samples of the 0.5% Pt/γ-Al_2O_3 catalyst and the γ-Al_2O_3 support material. The 5% Pt/γ-Al_2O_3 catalyst was kindly provided by Johnson-Matthey.

REFERENCES

1. Mann, R. F., Amphlett, J. C., and Peppley, B. A., *Frontiers Sci. Ser.* **7**, 613 (1993).
2. Daimler-Benz, A. G., "NECAR II—Driving without Emissions," Daimler-Benz, A. G., Stuttgart, Germany, 1996.
3. Murray, H. S., 1985 Fuel Cell Seminar, Book of Abstracts, *in* "Fuel Cell," p. 129, sponsored by the National Fuel Cell Coordinating Group, Tucson, AZ, 1985.
4. Kumar, R., and Ahmed, S., *in* "Proceedings of the First International Symposium on New Materials for Fuel Cell Systems, Ecole Poytechnique de Montreal, Montreal, 1995" (O. Savadogo, P. R. Roberge, and T. N. Veziroglu, Eds.), pp. 224–238.
5. Oetjen, H.-F., Schmidt, V. M., Stimming, U., and Trila, F., *J. Electrochem. Soc.* **143**, 3838 (1996).
6. Colsman, G., "Verfahrenstechnische Optimierung der Brenngaserzeugung für Brennstoffzellen in Kraftfahrzeugen," Disseration of the RWTH Aachen, 1995.
7. Lemons, R. A., *J. Power Sources* **29**, 251 (1990).
8. Brown, M. L., Green, A. W., Cohn, G., and Andersen, H. C., *Ind. Eng. Chem.* **52**, 841 (1960).
9. Cohn, J. G. E., U.S. Patent 3,216,782, Nov. 9, 1965.
10. Bonacci, J. C., Otchy, T. G., and Ackerman, T., U.S. Patent 4,238,468, Dec. 9, 1980.
11. Oh, S. H., and Sinkevitch, R. M., *J. Catal.* **142**, 254 (1993).
12. Plog, C., Maunz, W., Stengel, T., and Andorf, R., European Patent 0,650,922 A1, May 3, 1995.
13. Plog, C., Maunz, W., Stengel, T., and Andorf, R., European Patent 0,650,923 A1, May 3, 1995.
14. Watanabe, M., Uchida, H., Igarashi, H., and Suzuki, M., *Chem. Lett.* 21 (1995).
15. Nieuwenhuys, B. E., *in* "Elementary Reaction Steps in Heterogeneous Catalysis, Proceedings of the NATO Advanced Research Workshop, Bédoin, Vaucluse, France, Nov. 1992" (R. W. Joyner and R. A. van Santen, Eds.), p. 155, Kluwer Academic, Dordrecht, Netherlands, 1993.
16. Engel, T., and Ertl, G., *Adv. Catal.* **28**, 1 (1979).
17. Engel, T., and Ertl, G., *in* "The Chemical Physics of Solid Surfaces and Heterogeneous Catalysis" (D. A. King and D. P. Woodruff, Eds.), Vol. 4, p. 73, Elsevier Scientific, Amsterdam, 1982.
18. Rodriguez, J. A., and Goodman, D. W., *Surf. Sci. Rep.* **14**, 1 (1991).
19. Fuchs, S., Hahn, T., and Lintz, H.-G., *Chem. Eng. Proc.* **33**, 363 (1994).
20. Haaland, D. M., and Williams, F. L., *J. Catal.* **76**, 450 (1982).
21. Kahlich, M., Schubert, M. M., Hüttner, M., Noeske, M., Gasteiger, H. A., and Behm, R. J., *in* "Proceedings, 2nd International Symposium on New Materials for Fuel Cell and Modern Battery Systems" (O. Savadogo, Ed.), Ecole Poytechnique de Montreal, Montreal, in press.
22. Cant, N. W., *J. Catal.* **62**, 173 (1980).
23. Sarkany, J., and Gonzalez, R. D., *Appl. Catal.* **5**, 85 (1983).
24. Paål, Z., Schlögl, R., and Ertl, G., *J. Chem. Faraday Trans.* **88**, 1179 (1982).
25. Lööf, P., Stenbom, B., Norden, H., and Kasemo, B., *J. Catal.* **144**, 60 (1993).
26. Cant, N. W., Hicks, P. C., and Lennon, B. S., *J. Catal.* **54**, 732 (1978).
27. Cant, N. W., *J. Catal.* **74**, 411 (1982).
28. Cant, N. W., and Donaldson, R. A., *J. Catal.* **71**, 320 (1981).
29. Cant, N. W., and Angove, D. E., *J. Catal.* **97**, 36 (1986).
30. Schubert, M. M., Gasteiger, H. A., and Behm, R. J., submitted to *J. Catal.*
31. Levenspiel, O., "Chemical Reaction Engineering," Wiley, New York, 1972.
32. Barth, R., Pitchai, R., Anderson, R. L., and Verykios, E. V., *J. Catal.* **116**, 61 (1989).
33. Racine, B. N., Sally, J. J., Wade, B., and Herz, R. K., *J. Catal.* **127**, 307 (1991).
34. Altman, E. I., and Gorte, R. J., *J. Catal.* **110**, 191 (1988).
35. Altman, E. I., and Gorte, R. J., *Surf. Sci.* **172**, 71 (1986).
36. Winkelmann, F., Wohlrab, S., Libuda, J., Bäumer, M., Cappus, D., Menges, M., Al-Shamery, K., Kuhlenbeck, H., and Freund, H.-J., *Surf. Sci.* **307**, 1148 (1994).

37. Luo, J. S., Tobin, R. G., Lambert, D. K., Fisher, G. B., and DiMaggio, C. L., *Surf. Sci.* **274**, 53 (1992).
38. Hayden, B. E., Kretzschmar, K., and Bradshaw, A. M., *Surf. Sci.* **149**, 394 (1985).
39. Demmin, R. A., and Gorte, R. J., *J. Catal.* **90**, 32 (1984).
40. Yacamán, J. M., and Dominguez, E., *J. Catal.* **64**, 213 (1980).
41. Hollins, P., *Surf. Sci. Rep.* **16**, 51 (1992).
42. Jackman, T. E., Davies, J. A., Jackson, D. P., Unertl, W. N., and Norton, P. R., *Surf. Sci.* **120**, 389 (1982).
43. Norton, P. R., Davies, J. A., and Jackman, T. E., *Surf. Sci.* **122**, L593 (1982).
44. Anderson, J. A., *J. Chem. Faraday Trans.* **88**, 1197 (1992).
45. Bonzel, H. P., and Ku, R., *J. Vac. Sci. Technol.* **9**, 663 (1972).
46. Dabill, D. W., Gentry, S. J., Holland, H. B., and Jones, A., *J. Catal.* **53**, 164 (1978).
47. Demmin, R. A., and Gorte, R. J., *J. Catal.* **105**, 373 (1987).
48. Demmin, R. A., Ko, C. S., and Gorte, R. J., *J. Phys. Chem.* **89**, 1151 (1985).
49. Hardacre, C., Ormerod, R. M., and Lambert, R. M., *Chem. Phys. Lett.* **206**, 171 (1993).
50. Berlowitz, P. J., Peden, C. H. F., and Goodman, D. W., *J. Phys. Chem.* **92**, 5213 (1988).
51. Zafiris, G. S., and Gorte, R. J., *J. Catal.* **140**, 418 (1993).
52. Muraki, H., Matunaga, S.-I., Shinjoh, H., Wainwright, M. S., and Trimm, D. L., *J. Chem. Tech. Biotechnol.* **52**, 415 (1991).
53. Li, Y.-E., Boecker, D., and Gonzales, R. D., *J. Catal.* **110**, 319 (1988).
54. Henderson, M. A., and Yates, J. T. (Jr.), *Surf. Sci.* **268**, 189 (1992).
55. Wang, H., Tobin, R. G., and Lambert, D. K., *J. Chem. Phys.* **101**, 4277 (1991).
56. Wang, H., Tobin, R. G., Lambert, D. K., Fisher, G. B., and DiMaggio, C. L., *Surf. Sci.* **330**, 173 (1995).
57. Poelsema, B., Mechtersheimer, G., and Comsa, G., *Surf. Sci.* **111**, 519 (1981).
58. Ertl, G., Neumann, M., and Streit, K. M., *Surf. Sci.* **64**, 393 (1977).
59. Steininger, H., Lehwald, S., and Ibach, H., *Surf. Sci.* **123**, 264 (1981).
60. Parker, D. H., Fischer, D. A., Colbert, J., Koel, B. E., and Gland, J. L., *Surf. Sci.* **258**, 75 (1991).